Electronic Supplementary Material (ESI) for Dalton Transactions.
This journal is © The Royal Society of Chemistry 2023

Electronic Supplementary Information

Tin-doped $NiFe_2O_4$ Nanoblock Grown on Iron Foil for Efficient and Stable Water Splitting at Large-Current-Density

Juan Jian,[a] Meiting Wang,[a] Zhuo Wang,[a] Jingwen Meng,[a] Yuqin Yang[a] and Limin Chang[a,*]

[a] Key Laboratory of Preparation and Applications of Environmental Friendly Material of the Ministry of Education, College of Chemistry, Jilin Normal University, Changchun 130103, P. R. China

* Corresponding authors' E-mails: changlimin2139@163.com

1. Material and Experimental Instruments

1.1 Materials used in the experiment

RuO_2 was synthesized from ruthenium chloride hydrate ($RuCl_3 \cdot xH_2O$) purchased from Aladdin Ltd. (Shanghai, China).[1] Pt/C (20 wt%) was obtained from Macklin Ltd. (Shanghai, China), Nickel foam (NF) and iron foil (IF) were provided by the Li Yuan Technology Co. Ltd. (Shanxi, China). KOH, $Na_2SnO_3 \cdot 3H_2O$, HCl and other chemicals are supplied by the Beijing Chemical Reagents Company. Apart from the NF and IF, all the chemicals are analytical pure and do not needed further purification.

1.2 Experimental Section

Detailed Synthesis Information

Firstly, weighing 1.0 mmol thiourea and 0.19 mmol sodium stannate; then, mix them into 50 mL deionized water under continuous magnetic stirring; later, transferred the mixture solution into the polytetrafluoroethylene hydrothermal reactor; after that, place the acid treated NF (2 cm * 5 cm) and sanded IF (1 cm * 5 cm) into the autoclave; at last, reacted at 220 ^{o} oven for 5 hours. The finally gained IF based material is the Sn-$NiFe_2O_4$/IF and the doped mass percentage of Sn is 1.92 %. In addition, the synthesis path of $NiFe_2O_4$/IF was similar with the Sn-$NiFe_2O_4$/IF, just without the participation of sodium stannate.

Basic Phase Characterizations

X-ray diffraction (XRD) experiment was tested on a Rigaku D-Max 2550 diffractometer with Cu-Kα radiation (λ = 1.5418 Å). Scanning electron microscope (SEM) and energy dispersion X-ray spectroscopy (EDX) images were obtained on a JEOL-6700 scanning electron microscope. Transmission electron microscope (TEM), high resolution TEM (HRTEM) images were obtained with microscopy of Philips-FEI Tecnai G2S-Twin, equipped with a field emission gun operating at 200 kV. X-ray photoelectron spectra (XPS) analysis was performed on a VG Scienta R3000 spectrometer with Al Kα (1486.6 eV) as the X-ray source. Contact angle (CA) experiment was analyzed by the machine of Dataphysics OCA20 at room temperature.

Electrochemical Measurements

The electrochemical measurements were conducted using the three-electrode system with the electrochemical workstation (CHI 760e). The as-prepared electrodes were directly used as the working electrodes; meanwhile, graphite rod and Hg/HgO electrode were served as counter and reference electrodes, respectively. 1.0 M KOH solution was used as

electrolyte for HER, OER and OWS devices. Potentials were normalized versus the standard hydrogen electrode (RHE) according to formula below:

$$E_{(RHE)} = E_{(Hg/HgO)} + 0.098\ V + 0.0591\ pH \quad (1)$$

Here, "$E_{(Hg/HgO)}$" is the potential we directly measured during the experiment.

Polarization curves were performed via sweeping potentials at a scan rate of 2.0 mV s^{-1}. The measured potentials were calibrated with *iR* compensation. Corresponding stability data were examined through current-time curves at the constant potentials.

Tafel slope:

The data of Tafel slope can be plotted by the gained linear sweep voltammetry (LSV) curves, which is obtained from the follow equation:

$$\eta = a + b \log j \quad (2)$$

Where, "η" refers to the overpotential; "j" is the current density; "a" relates to the j_0 (exchange current density) and can be reflected by the intercept; "b" is the Tafel slope.

Electrochemical impedance spectroscopy (EIS):

We operated the ESI testing using the CHI 760e, frequency ranged from 1.0 to 100000 Hz, amplitude is 0.005 V.

Electrochemical active surface area (EASA):

The EASA was gained follow the formula below:

$$EASA = A * C_{dl} / C_s \quad (3)$$

Where "A" refers to the area of the working electrode, and we set the electrode area to 0.25 cm^2 throughout the electrocatalytic water splitting testing; "C_s" relates to the electrolyte, here C_s = 0.04 mF cm^{-2}; "C_{dl}" is the abbreviation of double layer capacitance and calculated from series of CV curves that tested within the non-Faraday potential range (0.9254-1.0254 V vs. RHE), scan rate changed from 10 to 100 mV s^{-1}, increased with 10 mV s^{-1} each time.

Faraday efficiency (FE):

Faraday efficiency (FE) of Sn-$NiFe_2O_4$/IF for OER/HER can be calculated by the ratio of the amount of O_2/H_2 collected by drainage method and the theoretical O_2/H_2. Take OER for example, the actual amount O_2 production (labeled as $n_{o\text{-}experimental}$) can be calculated using the equation of $n_{o\text{-}experimental} = V/V_m$, where V is the volume of O_2 collected from the chronoamperometry testing; V_m is molar volume of ideal gas, and V_m = 22.4 L mol^{-1}. For the theoretical O_2 (marked as $n_{o\text{-}theoretical}$) accumulated during the OER. According the OER

equation of $4OH^- \rightarrow O_2 + 2H_2O + 4e^-$, where, the electrolytic efficiency (η) can be measured by the equation of $\eta = z*n*F/Q$. Here, "n" is the mole of O_2 generated during the OER, and can be marked as $n_{o\text{-}theoretical}$; "z" is the number of transferred electrons generated per mole of O_2 during the OER, here, z = 4; "F" is the Faraday constant, F = 96485 C mol^{-1}; "Q" refers to the actual quantity of electric charge, and can be calculated by the flume of $Q = \Sigma i*t$. In the chronoamperometry experiment, the Q can be directly calculated. To evaluate the FE of a catalyst for OER, we assume that 100 % current efficiency occurs during the whole reaction. Hence, $1 = 4*F*n_{o\text{-}theoretical}/Q$, therefore, $n_{o\text{-}theoretical} = Q/(4*F)$. The calculation of FE for HER is similar with the OER, merely the the number of transferred electrons generated per mole of H_2 during the HER is 2.[2-4]

3. Supplementary Figures and Tables

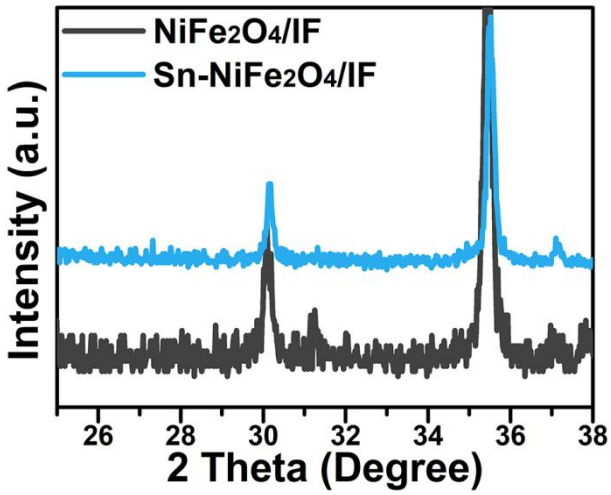

Fig. S1. Enlarged XRD image of $NiFe_2O_4$/IF and Sn-$NiFe_2O_4$/IF.

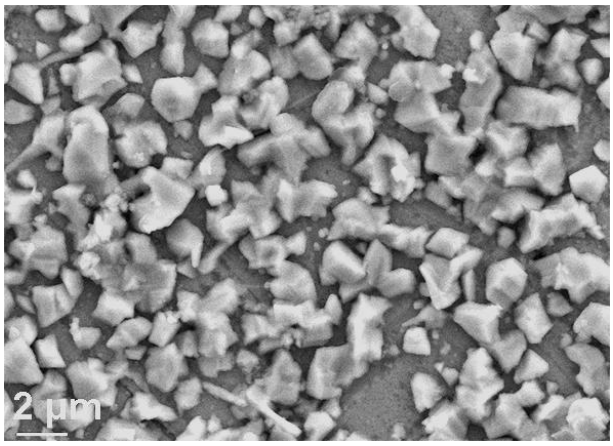

Fig. S2. SEM image of the pure $NiFe_2O_4$/IF.

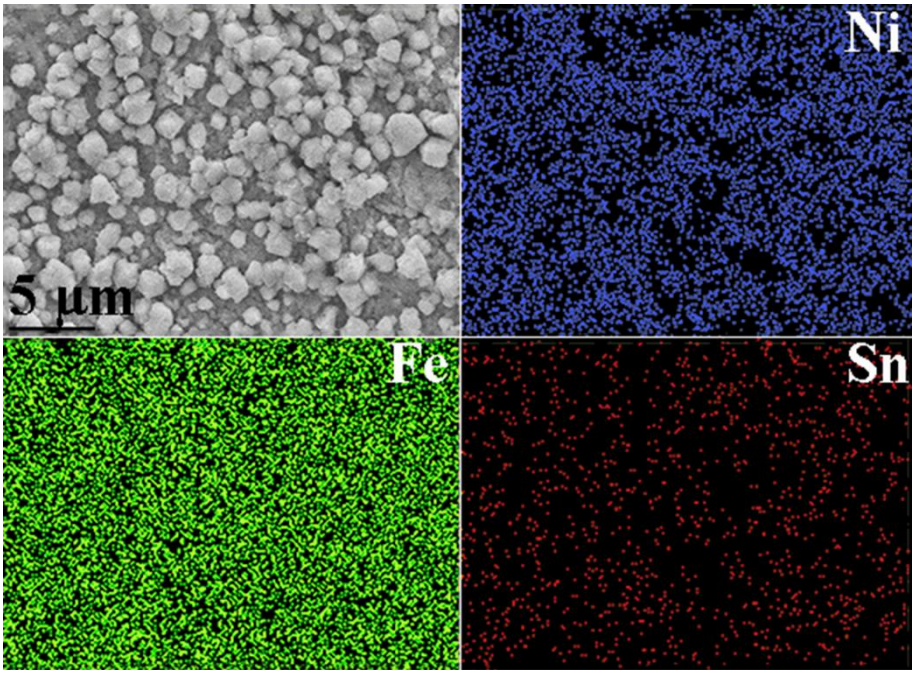

Fig. S3. EDX-Mapping (SEM) results of Ni, Fe, Sn in Sn-$NiFe_2O_4$.

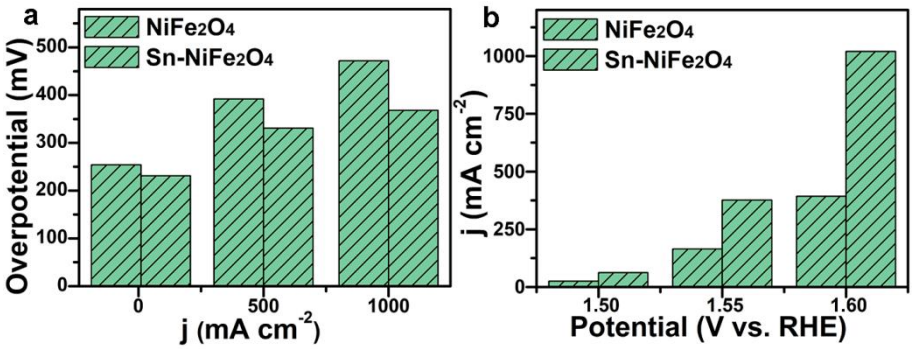

Fig. S4. The bar graph reflecting the relationship between current density and given potential of $NiFe_2O_4$/IF and Sn-$NiFe_2O_4$/IF for the OER course.

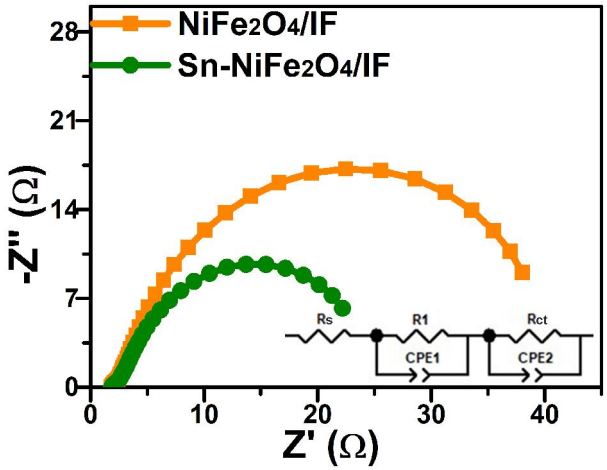

Fig. S5. The electrochemical impedance spectroscopy (EIS) curves of $NiFe_2O_4$/IF and Sn-$NiFe_2O_4$/IF at overpotential of 275 mV, insert is the equivalent circuit for fitting the Nyquist plots.

As illustrated in the equivalent circuit, R represents resistance. Here, R_s and R_{ct} refers to the resistance of solution and charge transfer, respectively. It is generally accepted that small R_{ct} values give rise to rapid charge transfer kinetics. Obviously, the Sn-$NiFe_2O_4$/IF (11.2 Ω) has much lower charge transfer resistance than the pure $NiFe_2O_4$/IF (19.4 Ω). Thus, the doped-Sn shortened the charge transfer path and accelerated the electrocatalytic reactions of Sn-$NiFe_2O_4$/IF.

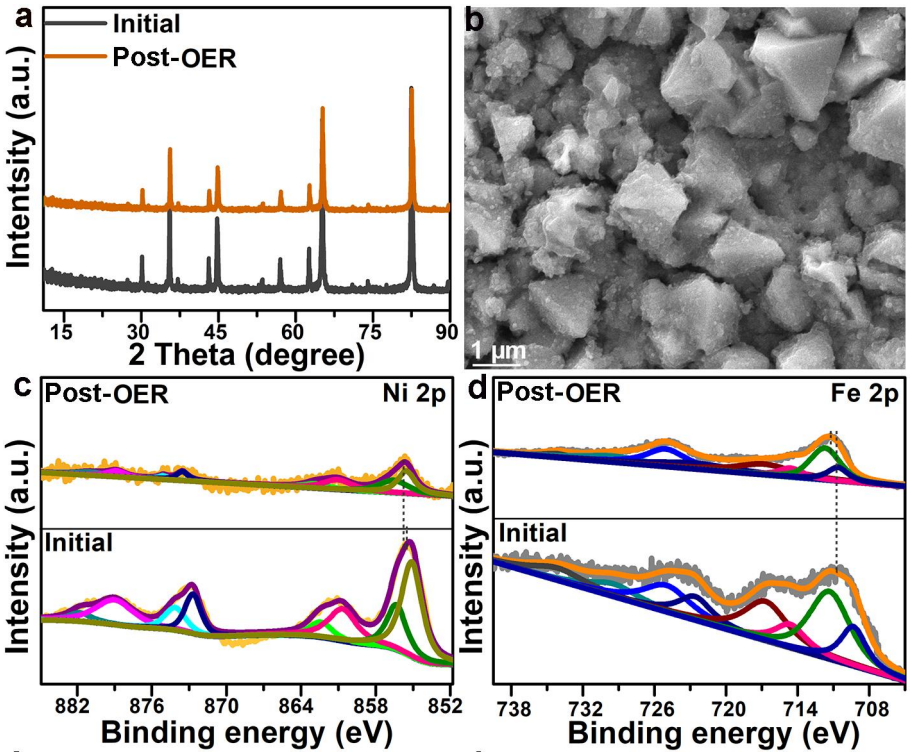

Fig. S6. The basic characterization results of (a) XRD, (b) SEM and (c, d) XPS data of Ni 2p, Fe 2p that post-OER for Sn-$NiFe_2O_4$/IF.

The slightly high binding energy shift of Ni 2p and Fe 2p after the OER, which maybe due to the accumulation of oxyhydroxide species.[5,6]

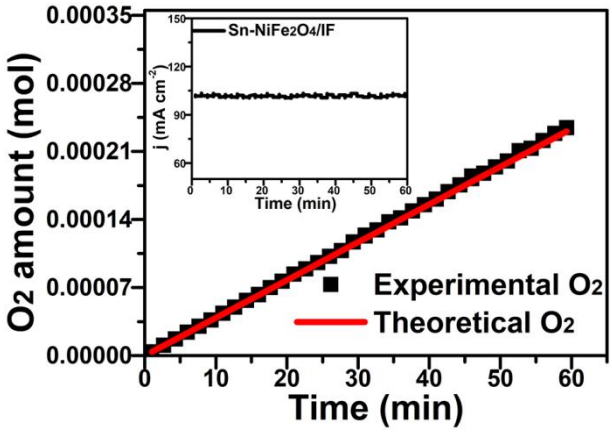

Fig. S7. Faraday efficiency image of Sn-$NiFe_2O_4$/IF during the OER course, the insert graph is the corresponding i-t test.

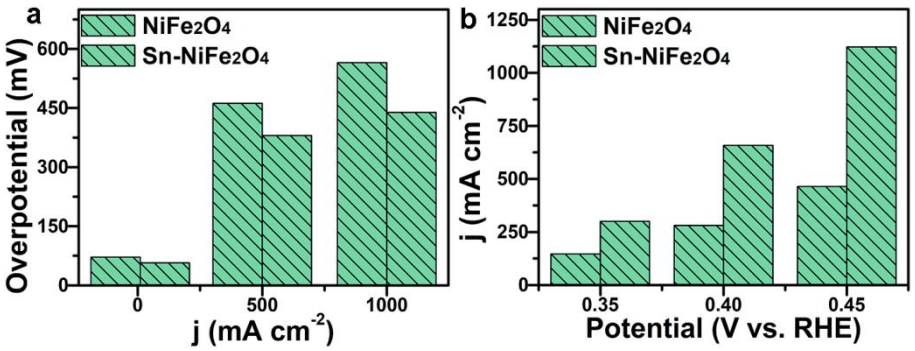

Fig. S8. The bar graph reflecting the relationship between current density and given potential of $NiFe_2O_4$/IF and Sn-$NiFe_2O_4$/IF for the HER process.

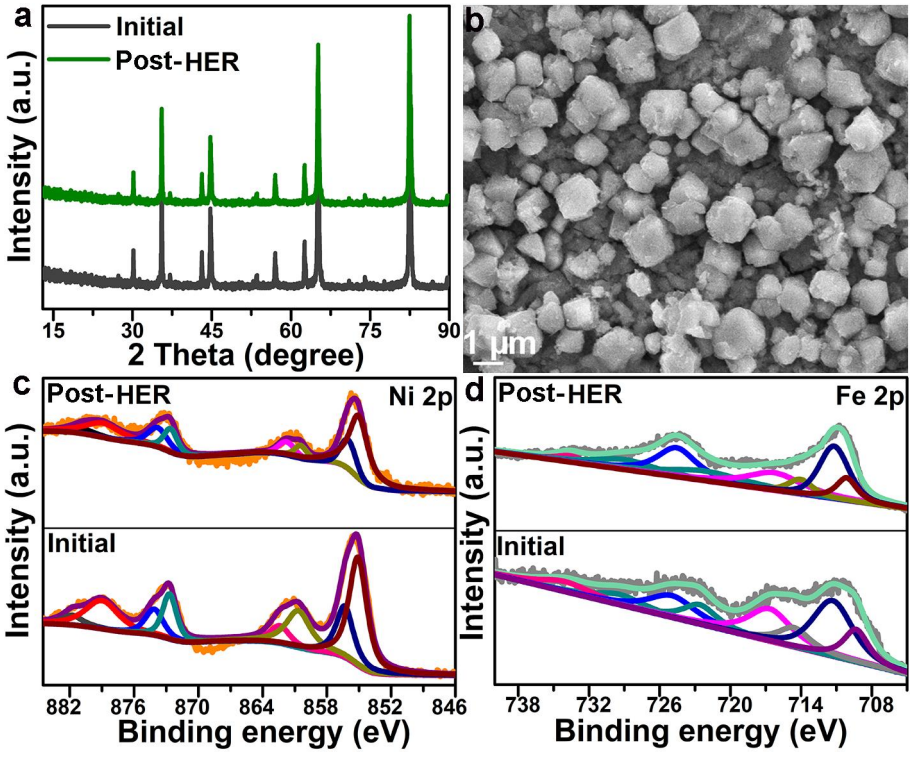

Fig. S9. The basic characterization results of (a) XRD, (b) SEM and (c, d) XPS data of Ni 2p, Fe 2p that post-HER for Sn-$NiFe_2O_4$/IF.

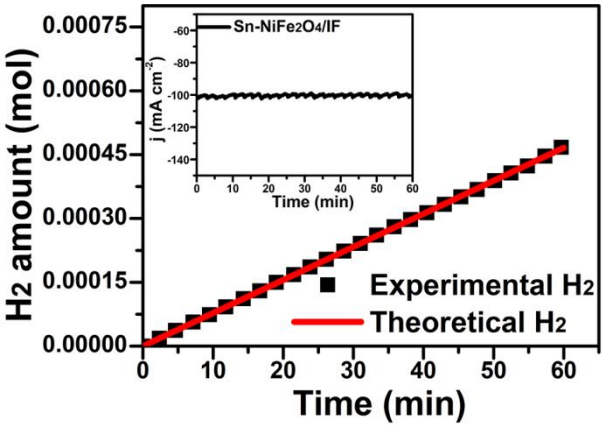

Fig. S10. Faraday efficiency result of Sn-$NiFe_2O_4$/IF for HER, wherein the insert image is the corresponding i-t curves.

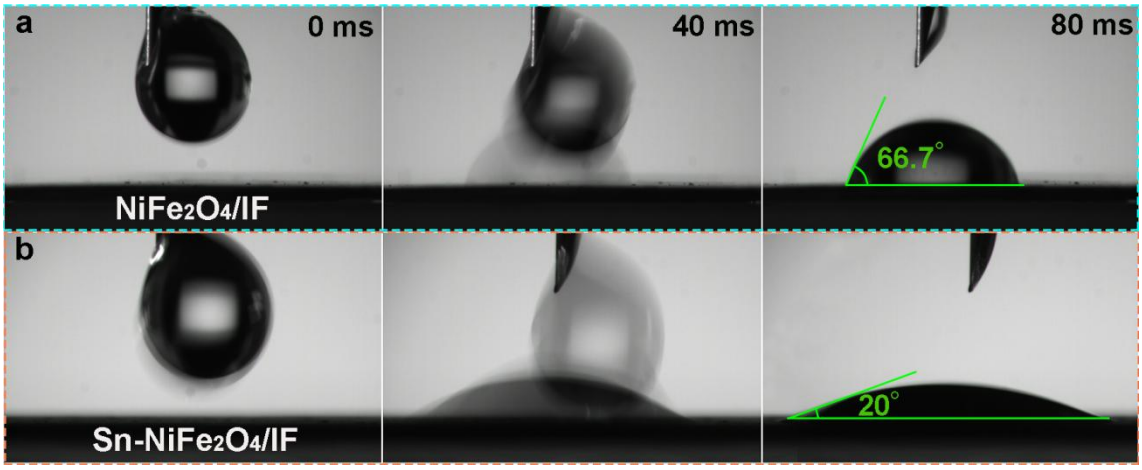

Fig. S11. Contract angle experiment of (a) $NiFe_2O_4$/IF and (b) Sn-$NiFe_2O_4$/IF at measure time of 0, 40 and 80 ms.

Table S1. A properties comparison of various electrocatalysts for overall water splitting (OWS).

Catalys (OWS)	Voltage at 10 mA cm^{-2} (V)	Voltage at 100 mA cm^{-2} (V)	Reference
Sn-$NiFe_2O_4$/IF	1.56	1.80	This work
$NiFe_2O_4$/IF	1.68	1.94	This work
Pt/C‖RuO_2	1.56	1.81	This work
Fe_2O_3/Ni_3S_2	1.54	≈1.81	[7]
CoMoP	1.56	1.70	[8]
S-$NiFe_2O_4$/Ni_3Fe/NW	1.52	1.79	[9]
Co/CNFs	1.60	——	[10]

$Co_9S_8/Ni_3S_2/NF$	1.64	——	[11]
CoMoO nanosheet arrays@NF	1.68	≈1.88	[12]
Ni_3FeN/r-GO	1.60	≈1.96	[13]
P-Co_3O_4/NF	1.63	——	[14]
CoP@3D Ti_3C_2-Mxene	1.57	≈1.70	[15]
P-doped Co-Ni-S/NF	1.60	——	[16]
RuO_2/NiO/NF	1.50	——	[17]
Fe-Ni_2P	1.49	≈1.73	[18]
Ni_3S_2-NGQDs/NF	1.58	——	[19]
NiFe/$Ni(OH)_2$/NiAl	1.59	——	[20]
MoP/Ni_2P/NF	1.55	——	[21]
N(P)-doped 304-type stainless steel mesh	1.74	——	[22]
Cu@CoS_x/Cu Foam	1.50	1.80	[23]
CoFePO/NF	1.56	≈1.95	[24]
N-Ni_3S_2/ NF	1.48	≈1.83	[25]
$NiCo_2S_4$ nanowire arrays	1.63	——	[26]
NiFeOOH	——	1.49	[27]
CP/CTs/Co-S	1.74	——	[28]
NiCoP	1.58	≈1.81	[29]
CoFeZr oxides/NF	1.63	≈1.80	[30]
MoS_2-NiS_2/NGF	1.64	——	[31]
Ni-graphitic carbon (NGC)	1.64	——	[32]
MoO_3/Ni-NiO	1.55	——	[33]
Ni@NC800/NF	1.60	——	[34]
$Ni_{1-x}Fe_x$/NC/NF	1.58	——	[35]

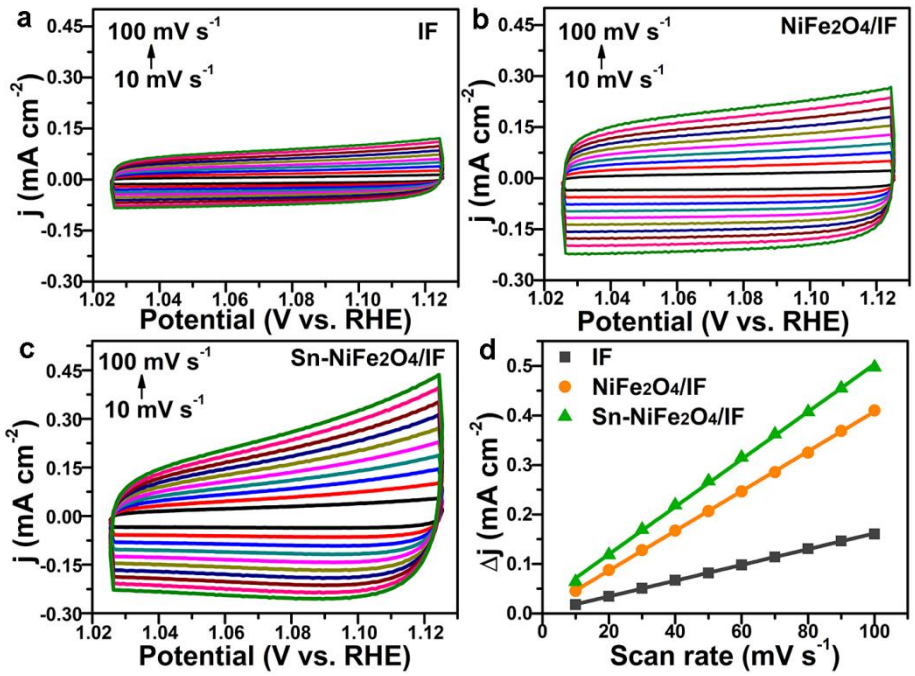

Fig. S12. CV curves at different scan rates of (a) IF, (b) $NiFe_2O_4$/IF, (c) Sn-$NiFe_2O_4$/IF and their (d) relationship curves between Δj and scan rates.

Table S2. Information of C_{dl}, C_s and EASA of the IF, $NiFe_2O_4$/IF and Sn-$NiFe_2O_4$/IF.

	IF	**$NiFe_2O_4$/IF**	**Sn-$NiFe_2O_4$/IF**
Fitted slope (mF cm^{-2})	0.0016	0.0041	0.0048
Standard error for slope	$8.64*10^{-6}$	$1.75*10^{-5}$	$4.75*10^{-5}$
Double-layer-capacitance (C_{dl}, mF cm^{-2})	0.80	2.05	2.40
General specific capacitance (C_s, mF cm^{-2})	0.04	0.04	0.04
Electrochemical active surface area (EASA, cm^2)	5.00	12.8	15.0

4. Reference

[1] Jian, J.; Yuan, H. M.; Feng, S. H. et al. *ACS Appl. Mater. Inter.,* **2018**, 10, 40568.

[2] Liu, Y. P.; Zou, X. X. et al, *Nat. Commun*., **2018**, 9, 2609.

[3] Suryanto, B. H. R.; Zhao, C. et al, *Nat. Commun*., **2019**, 10, 5599.

[4] Zou, X. X.; Zhang Y. *Chem. Soc. Rev.*, **2015**, 44, 5148-5180.

[5] Liu, J. L.; et al. *Chem. Commun.*, **2019**, 55, 10860-10863.

[6] Liu, Z.; et al. *Chem. Eng. J.*, **2020**, 395, 125170.

[7] Shao, Z. Y.; Wang, Q. *Chem. Eng. J.,* **2021**, 416, 129098.

[8] Wang, X.; Cabot, A. *Nanomaterials,* **2022**, 12, 1098.

[9] Gao, M. Y.; Xu, C. Y. *J. Mater. Chem. A*, **2018**, 6, 1551-1560.

[10] Yang, Z. K.; Li, Y. D. et al. *Adv. Mater.*, **2019**, 31, 1808043.

[11] Du, Feng.; Shi, L.; Zou, Z. G. et al. *Appl. Catal., B* **2019**, 253, 246.

[12] Zhang, Y.; Shao, Q.; Huang, X. Q. et al. *Nano Energy,* **2018**, 45, 448.

[13] Gu, Y.; Chen, S.; Yao, X. D. et al. *ACS Nano,* **2018**, 12, 245.

[14] Wang, Z. C.; Liu, H. L.; Sun, X. P. et al. *ACS Catal*., **2018**, 8, 2236.

[15] Xiu, L. Y.; Wang, Z. Y.; Qiu, J. S. et al. *ACS Nano,* **2018**, 12, 8017.

[16] Zhang, F. F.; Ge, Y. C.; Shen, J. F. et al. *ACS Appl. Mater. Inter.,* **2018**, 10, 7087.

[17] Liu, J. S.; Zheng, Y.; Qiao, S. -Z. et al. *Small,* **2018**, 14, 1704073.

[18] Li, Y. J.; Zhang, H. C.; Sun, X. M. et al. *Adv. Funct. Mater*., **2017**, 27, 1702513.

[19] Lv, J. J.; Zhao, J.; Zhu, J. J. et al. *Small,* **2017**, 13,1700264.

[20] Niu, S.; Jiang, W. -J.; Hu, J. -S. et al. *Adv. Sci*., **2017**, 4, 1700084.

[21] Du, C. C.; Shang, M. X.; Song W. B. et al. *J. Mater. Chem. A*, **2017**, 5, 15940.

[22] Balogun, M. -S.; Qiu, W. T.; Tong, Y. X. et al. *Adv. Mater*., **2017**, 1702095.

[23] Liu, Y. P.; Li, Q. J.; Zou, X. X. et al. *Adv.Mater*., **2017**, 29, 1606200.

[24] Duan, J. J.; Chen, S.; Qiao, S. Z. et al. *ACS Nano,* **2016**, 10, 8738.

[25] Chen, P. Z.; Zhou, T. P.; Xie, Y. et al. *Adv. Mater*., **2017**, 29, 1701584.

[26] Sivanantham, A.; Ganesan, P.; Shanmugam, S. *Adv. Funct. Mater*., **2016**, 26, 4661.

[27] Zhou, H. Q.; Yu, F.; Ren, Z. F. et al. *Energy Environ. Sci*., **2018**, 11, 2858.

[28] Wang, J.; Zhong, H. -X.; Zhang, X. -B. et al. *ACS Nano,* **2016**, 10, 2342.

[29] Liang, H. F.; Gandi, A. N.; Alshareef, H. N. et al. *Nano Lett.,* **2016**, 16, 7718.

[30] Huang, L. L.; Chen, D. W.; Wang, S. Y. et al. *Adv. Mater*., **2019**, 1901439.

[31] Kuang, P. Y.; He, M.; Fan, K. et al. *Appl. Catal., B,* **2019**, 254, 15.

[32] Zhou, B. H.; Zhang, M. C.; Zhang, Y. Y. et al. *Carbon,* **2019**, 150, 21.

[33] Li, X. P.; Wang, Y.; Hu, W. B. et al. *Adv. Mater.,* **2020**, 32, 2003414.

[34] Xu, Y.; Tu, W. G.; Xu, R. et al. *Adv. Mater*., **2017**, 29, 1605957.

[35] Zhang, X.; Xu, H. M.; Liang, Y. Y. et al. *ACS Catal*., **2016**, 6, 580.